Journal of Fluids and Structures (2001) **15,** 415–425
doi:10.1006/jfls.2000.0360, available online at http://www.idealibrary.com on IDEAL®

ASPECTS OF FLOW-INDUCED VIBRATION

A. Leonard and A. Roshko

Graduate Aeronautical Laboratories, California Institute of Technology
Pasadena, CA 91125, U.S.A.

(Received 20 September 2000, and in final form 22 November 2000)

Phenomena associated with flow-induced transverse oscillation of an elastically mounted body are considered. The use of a recently introduced parameter that combines the effect of mass and elasticity—effective elasticity—is exploited to demonstrate the predictive value of the new approach and to provide insights into solution branching, the maximum amplitude of vibration, and modeling.

1. INTRODUCTION

In Shiels, Leonard & Roshko (2001), henceforth SLR, results of numerical simulations were presented for vortex-induced vibration of a circular cylinder vibrating transversely in a two-dimensional flow at Reynolds number $\mathrm{Re} = 100$. The single value of Re together with zero value for the system damping ($b = 0$) were chosen, thus reducing the number of independent variables to two, namely the mass m and the spring constant k. It was found that, in a great majority of the cases, the response was essentially sinusoidal. In this situation, at frequency $f = \omega/2\pi$, the spring force, ky, and inertial force, $m\omega^2 y$, are continually in opposition, and their net effect can be represented by the "effective" elasticity, $k^*_{\mathrm{eff}} \equiv k^* - m^*\omega^{*2}$. The notation ()* indicates nondimensional forms,

$$k^* \equiv k/\tfrac{1}{2}\rho U_\infty^2, \quad m^* \equiv m/\tfrac{1}{2}\rho D^2, \quad \omega^* \equiv \omega D/U_\infty \quad \text{and } A^* \equiv A/D, \tag{1}$$

where ρ and U_∞ are flow density and velocity, respectively, and D is the cylinder diameter, i.e., the scaled time is $t^* = tU_\infty/D$ rather than the traditional $\tau \equiv t\omega_n$, where $\omega_n = (k/m)^{1/2}$. Scaling with flow variables instead of the mechanical ones leads to the single-variable formulation, which gives a unified solution as function of k^*_{eff}. In the traditional formulation, m^* is an independent parameter and the mechanical frequency ω_n appears in the "reduced velocity", $U_R \equiv U_\infty/\omega_n D$, that is usually adopted as the primary variable. It may also be writtten $U_R = 1/\omega^*_n$. In Figure 1, we show the results of numerical simulations for the response of the system A^* and $f^* = \omega^*/2\pi$ versus k^*_{eff}. The simulations are those reported in SLR and more recent ones by L. Barba (private communication).

The advantage of a universal solution in terms of a single parameter, k^*_{eff}, is that it is not necessary to make an experimental (computational) run for each value of m^*. On the other hand, the effect of mechanical parameters is hidden in the solution. For example, the phenomena of "lock-in" and of multiple branches which are observed in the conventional coordinates are not obvious. One of the main objectives of this paper is to elucidate the connection between these phenomena and our unified description.

The universal solution includes the transverse force ("lift") on the cylinder which, for sinusoidal motion, can be expressed as $F_y = C_L \tfrac{1}{2}\rho U_\infty^2 D \sin \omega t$. The coefficient C_L may be of

0889–9746/01/040415 + 11 $35.00/0.

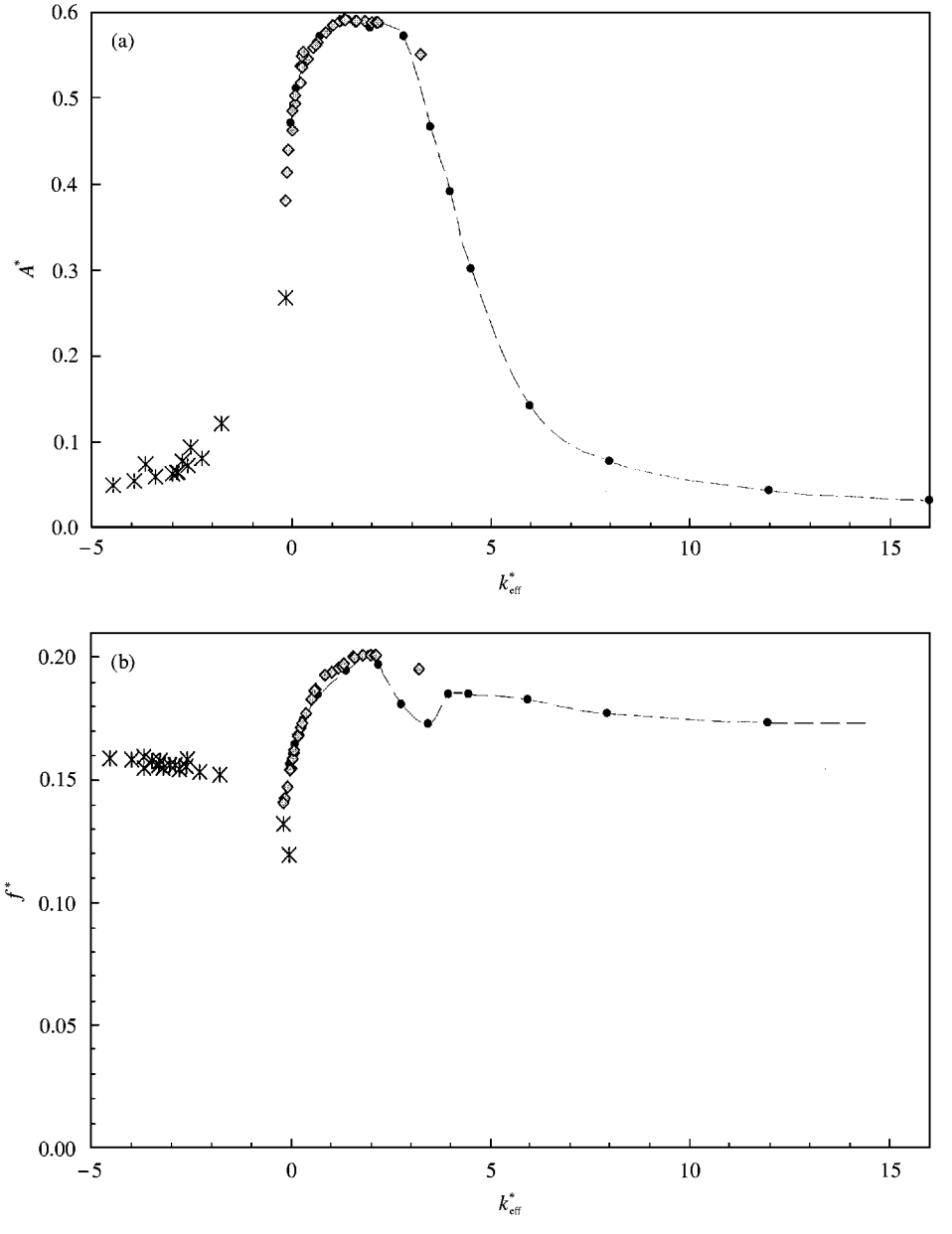

Figure 1. Response for undamped systems, with and without inertia, plotted against effective elasticity: (a) amplitude A^*; (b) frequency f^*. Notation: —●—, DS '98; ◇, LB '99; -×- LB '00. Numerical simulations of SLR (DS '98) and L. Barba (private communication, LB '99; '00).

interest for modeling. In SLR, the transverse force was decomposed into two components, $C_L = C_{Lw} + C_{La}$, where C_{Lw} is the "wake" force due to the effect of all the vorticity in the boundary layer and wake, while C_{La} is the "added-mass" force induced by the acceleration of the cylinder. The latter is easily computed for a given frequency and amplitude, i.e., $C_{La} = \frac{1}{2}\pi\omega^{*2}A^*$. Because of continuing controversy about the applicability of the classical result for the added mass contribution to the fluid force, we present a review in the

appendix. More difficult to understand is the total cross-force C_L and its component C_{Lw}. For example, it is counter-intuitive that $C_L = 0$ at the synchronization condition $f = f_n$, at which condition, then, $C_{Lw} = -C_{La}$. These aspects of the transverse force are described in Sections 2 and 3, while the branching solutions associated with the universal solution are discussed in Section 4.

2. SYNCHRONIZATION AND LOCK-IN

The two terms, synchronization and lock-in, are often used synonymously but in SLR it was shown that, for zero damping and sinusoidal motion, synchronization ($f = f_n$) occurs at only one condition, $k^*_{\text{eff}} = 0$. This follows from

$$k^*_{\text{eff}} = k^* - m^*\omega^{*2} = m^*(\omega^{*2}_n - \omega^{*2}), \tag{2}$$

which can be rewritten to show

$$\omega^{*2} = \omega^{*2}_n - k^*_{\text{eff}}/m^*. \tag{3}$$

That is, for nonzero values of k^*_{eff}, ω only approaches ω_n asymptotically when $m^* \gg 1$. Indeed, it is from experiments in air (Feng 1968), for which $m^* \sim 10^3$, that the traditional knowledge of "lock-in" developed. (Note, in equation (2), that in the range of high-amplitude response, $\omega^*_n = U_R^{-1} \sim 1$ and $k^*_{\text{eff}} < 3$.) On the other hand, it was from experiments in water [e.g., Khalak & Williamson (1997), Gharib *et al.* (1997), 1998, Gharib (1999)], for which $m^* \sim 1 - 10$, that the notion of "absence of lock-in" developed. In such cases, the plot of f/f_n is an increasing function of U_R which crosses the ordinate $f/f_n = 1$ at $U_R \approx 1{\cdot}0$. Those values of U_R for synchronization, at $\text{Re} \sim 10^3$–10^4, are remarkably close to the value from the universal solution $f^*(k^*_{\text{eff}})$ at $\text{Re} = 100$; that is, $f^*_n = f^*(0), = 0{\cdot}156$, from which $U_R = (2\pi f^*_n)^{-1} = 1{\cdot}02$.

It is also noteworthy that for large values of m^*, for which the synchronization value of U_R cannot be readily identified, as noted above, the value $U_R \approx 1{\cdot}0$ is the point at which a jump in amplitude is observed from an upper to a lower branch, as U_R is increasing. In some cases (Feng 1968; Brika & Laneville 1993), the jump is hysteretic, i.e., a jump from a lower to an upper branch, for decreasing U_R, is not observed. In other cases (Khalak & Williamson 1999), the jumps are intermittent rather than hysteretic, perhaps depending on the mass-damping parameter $m^*\zeta\,(= \frac{1}{2} U_R b^*)$. The connection with synchronization may be found in the equation of motion which, for zero damping and sinusoidal motion, as explained above, reduces to

$$(-m^*\omega^{*2} + k^*)A^* = k^*_{\text{eff}} A^* = C_{\text{L}}. \tag{4}$$

Thus, $C_L = m^*(\omega^{*2}_n - \omega^{*2})A^*$ is changing sign, i.e., phase, at synchronization. From the investigations in air ($m^* \gg 1$), it is known that at the hysteretic jump there is a phase change (π) in vortex shedding. Further discussion on branching is in Section 4.

3. AMPLITUDE AND CROSS-FORCE

To associate the amplitude of vibration A^* with the transverse force coefficient C_L can be misleading. Thus, for a stationary cylinder, $A^* = 0$ and $C_L = 1{\cdot}30$ while for a cylinder vibrating at high amplitude C_L may have the value zero (at $k^*_{\text{eff}} = 0$, where $A^* = 0{\cdot}47$!) Figure 2(a) shows the overall relation between C_L and A^*. The components of C_L, i.e., the added-mass component C_{La} and the wake component C_{Lw}, are shown in Figures 2(b) and 2(c), respectively. Clearly, the relations are not simple. The plot for the wake force is especially interesting, showing a large change of C_{Lw}, from negative to positive values, at

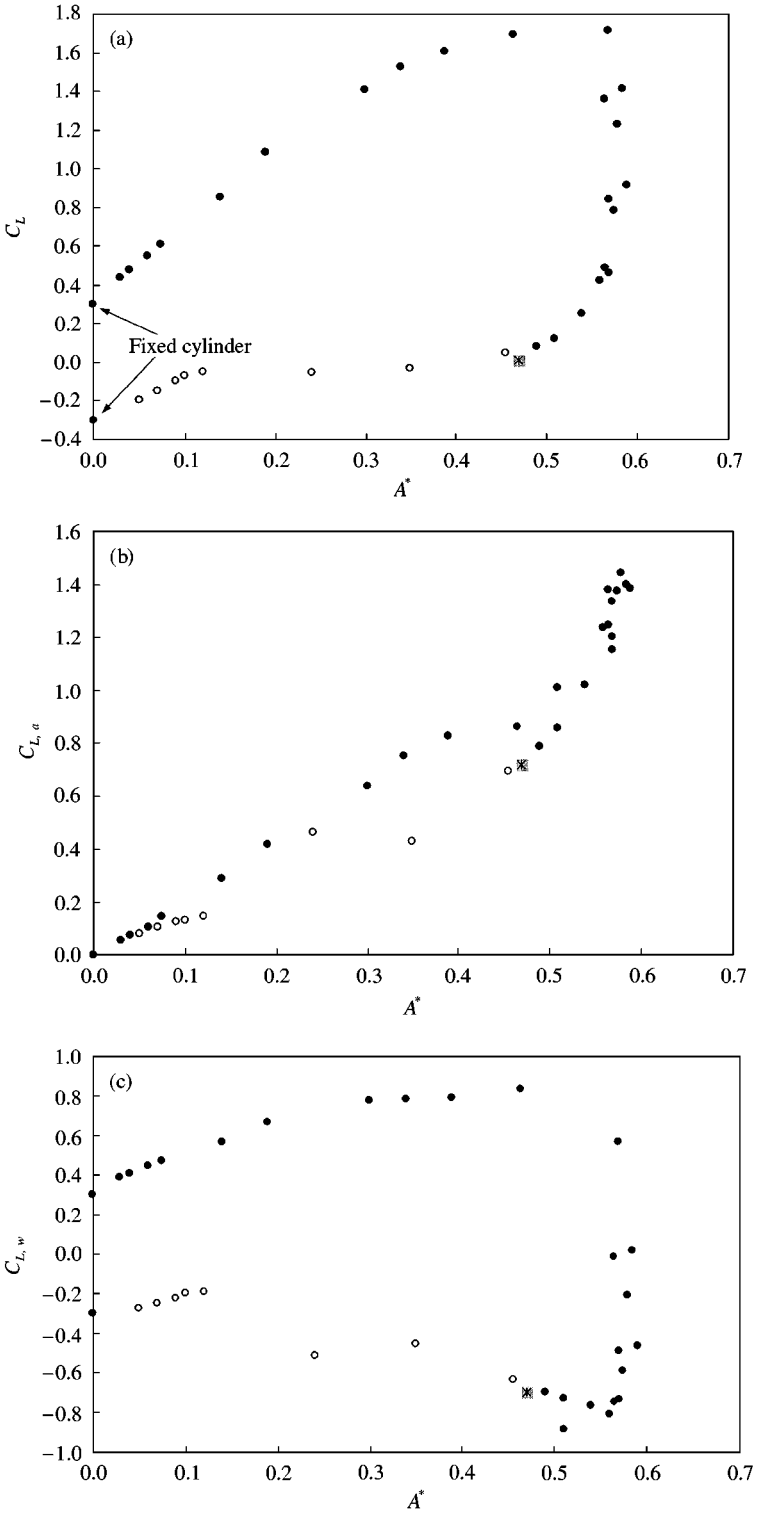

Figure 2. Components of the lift coefficient, $C_L = C_{La} + C_{Lw}$: (a) C_L; (b) C_{La} ; (c) C_{Lw}. Notation: ○ $k^*_{\text{eff}} < 0$; ● $k^*_{\text{eff}} > 0$; ⊠, $k^*_{\text{eff}} = 0$. Numerical simulations of SLR.

nearly constant amplitude, $A^* \approx 0{\cdot}58$. Surprisingly, as noted in SLR, that change is accompanied by barely perceptible change in the pattern of separation and vortical structure in the wake.

4. BRANCHING OF SOLUTIONS

In this section, we discuss the discontinuous or branching behavior often observed when following the amplitude of the response as the reduced velocity is varied continuously; see, e.g., Khalak & Williamson (1999). In particular, we show how this behavior is connected to our unified description.

As shown in Figure 1, the frequency, f^*, and amplitude, A^*, of the response will depend only on the effective stiffness, $k^*_{\text{eff}} = k^* - m^*\omega^{*2}$, the nondimensional damping, b^*, and the Reynolds number, Re, i.e.,

$$f^* = f^*(k^*_{\text{eff}}, b^*, \text{Re}), \quad A^* = A^*(k^*_{\text{eff}}, b^*, \text{Re}), \tag{5, 6}$$

assuming that the motion is nearly sinusoidal. Given the functions (5) and (6), consider now determining the response for a given experiment. For a fixed mechanical and fluid system, m^* is fixed but k^*, b^*, and Re vary as the freestream velocity, U_∞, varies. If we then also fix U_∞, then we need only to solve equation (5) implicitly for f^* or $\omega^{*2} = 4\pi^2 f^{*2}$. To do so let

$$\omega^{*2} = F(k^*_{\text{eff}}, b^*, \text{Re}). \tag{7}$$

Then

$$k^*_{\text{eff}} = k^* - m^*\omega^{*2} = k^* - m^*F(k^*_{\text{eff}}, b, \text{Re}). \tag{8}$$

Thus

$$m^*F(k^*_{\text{eff}}, b^*, \text{Re}) + k^*_{\text{eff}} = k^* = \frac{m^*}{U_R^2}, \tag{9}$$

and so k^*_{eff} may be determined from (9) and then f^* or ω^{*2} may be found from equations (5) or (7), respectively, and A^* from (6). (An alternative procedure to do this inversion was presented in SLR in which one begins with chosen m^* and k^*_{eff} and then determines the corresponding A^*, f^* and U_R. However, using this method it is not convenient to demonstrate branching behavior and one also has accuracy problems at large m^* as discussed by SLR.)

However, equation (9) may produce multiple solutions for k^*_{eff}. Consider the data produced by computational experiments of SLR for $b^* = 0$ and $\text{Re} = 100$. Using the results shown in Figure 1, we show in Figure 3 the left-hand side of equation (9) versus k^*_{eff} for the case $m^* = 2$. Note that, in this case, any value of U_R will produce a unique value k^*_{eff}, i.e., no multiple solutions. On the other hand, as m^* increases the importance of the nonlinear (in k^*_{eff}) first term on the left-hand side of equation (9) increases. For example the case $m^* = 28$ is shown in Figure 4. Note that in the range $36 \leq m^*/U_R^2 \leq 46$ or $0{\cdot}78 \leq U_R \leq 0{\cdot}88$ three solutions may be possible. As illustrated in the figure, the one corresponding to the largest k^*_{eff} would have the lowest amplitude [see Figure 1(a)] and therefore belong to the "lower" branch and the smallest k^*_{eff} would correspond to the highest amplitude or "upper" branch. A third or intermediate solution could possibly fall in the range $2 \leq k^*_{\text{eff}} \leq 4$ but it is approximately within this range that the response has been found to be nonsinusoidal as indicated in the figure. Branching for this case ($m^* = 28$) is seen to occur also in the range $16 \leq m^*/U_R^2 \leq 25$ or $1{\cdot}06 \leq U_R \leq 1{\cdot}32$ and corresponds to the branching discussed in Section 3, connected with the condition $k^*_{\text{eff}} \approx 0$. In this regime the largest solution for

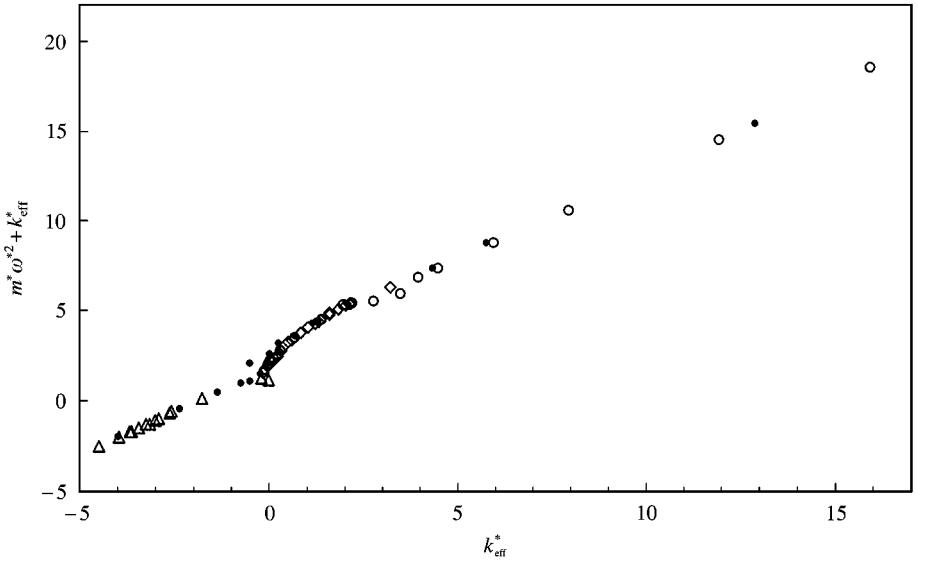

Figure 3. $m^*\omega^{*2} + k^*_{\text{eff}}$ or m^*/U^2_R plotted against effective elasticity for the case $m^* = 2.0$: ○, DS, $m = 0$; ●, DS, $m \neq 0$; ◇, LB '99; △, LB '00. Numerical simulations of SLR and L. Barba (private communication).

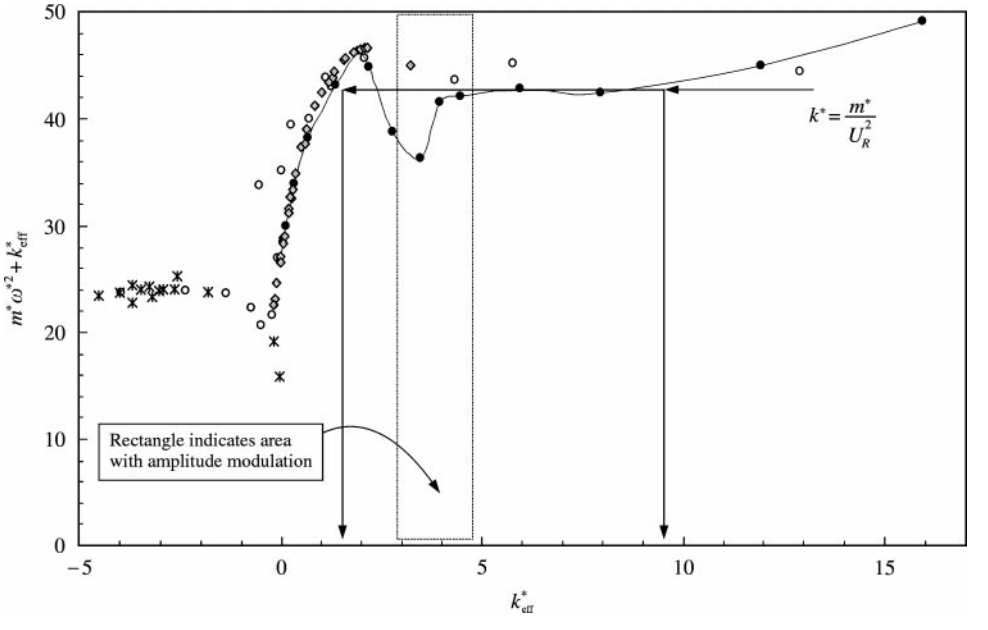

Figure 4. $m^*\omega^{*2} + k^*_{\text{eff}}$ or m^*/U^2_R plotted against effective elasticity for the case $m^* = 28.0$: ○, DS, $m = 0$; —●—, DS, $m \neq 0$; ◇, LB '99; △, LB '00. Numerical simulations of SLR and L. Barba (private communication).

k^*_{eff} (i.e., $k^*_{\text{eff}} \approx 0$) would correspond to the largest amplitude A^* while the intermediate solution for k^*_{eff} would yield, in general, a significantly smaller amplitude. A third solution also exists for a larger negative value of k^*_{eff}, because the left-hand side of equation (9) tends to k^*_{eff} as k^*_{eff} becomes large negative, but the corresponding amplitude would be even smaller.

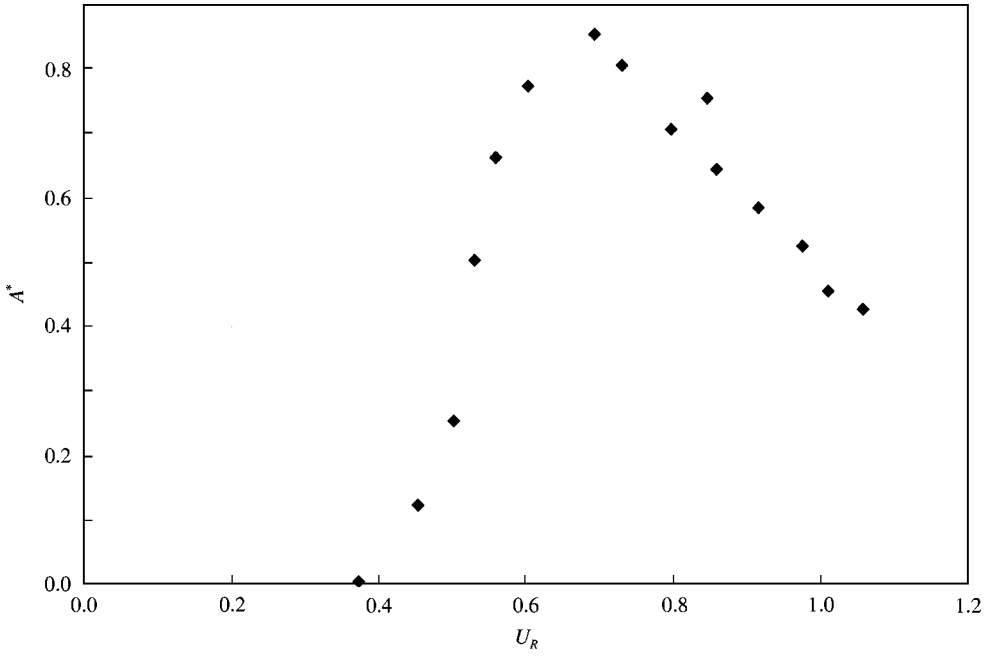

Figure 5. Amplitude plotted against reduced velocity for $m^* = 2{\cdot}1$. From the value $U_R = 1$: $b^* = 0{\cdot}31$, $k^* = m^*$, and $\mathrm{Re} = 32 \times 10^3$. Experiments of Gharib (1999).

This type of discontinuous or branching behavior is also found in the laboratory experiments of Gharib (1999), depending on the value of m^*. In Figure 5, we show the response A^* versus U_R, for the case $m^* = 2{\cdot}1$. A^* appears to vary smoothly, in agreement with the behavior inferred for the computational case, $m^* = 2$, from Figure 3. However, a different result occurs for the case $m^* = 28$, as shown in Figure 6. Note the nearly discontinuous behavior at $U_R \approx 0{\cdot}86$ and possible branching near $U_R \approx 1{\cdot}05$. The source of this behavior is clear when we consider the variation of $m^*F(k^*_{\mathrm{eff}}, b^*, \mathrm{Re}) + k^*_{\mathrm{eff}}$ as a function of k^*_{eff} for this data, shown in Figure 7. The jump in amplitude at $U_R \approx 0{\cdot}86$ is a consequence of the flatness of the curve in the range $4 \leq k^*_{\mathrm{eff}} \leq 6$ and the fact that A^* is a rapidly varying function of k^*_{eff} in this range (see Figure 8). The drop to low A^* at $U_R \approx 1{\cdot}05$ is simply the change in solution branch as m^*/U_R^2 decreases through the value ≈ 25.

In the laboratory experiments (fixed m^* but U_R variable) some variation in b^* and Re takes place because $b^* \sim U_R^{-1}$ and $\mathrm{Re} \sim U_R$. [For the case $m^* = 2{\cdot}1$ above, $b^* = 0{\cdot}31$ and $\mathrm{Re} = 32 \times 10^3$ at $U_R = 1$ and, for the case $m^* = 28$, $b^* = 0{\cdot}39$ and $\mathrm{Re} = 23 \times 10^3$ at $U_R = 1$ (Gharib 1999).] Thus, the data shown in Figure 7 are not at fixed b^* and Re, but include some variation in both parameters while the data of Figures 3 and 4 are at fixed $b^* = 0$ and $\mathrm{Re} = 100$. Of course, equation (9) is valid in either case but its use in the case of varying b^* and Re may require some additional iteration.

5. REMARKS

We have developed further insights into the phenomena of flow-induced vibration by exploiting a unified description of the response of the system, presented in a recent paper by SLR. In this approach, the effective elasticity, k^*_{eff}, and damping, b^*, replace three traditional

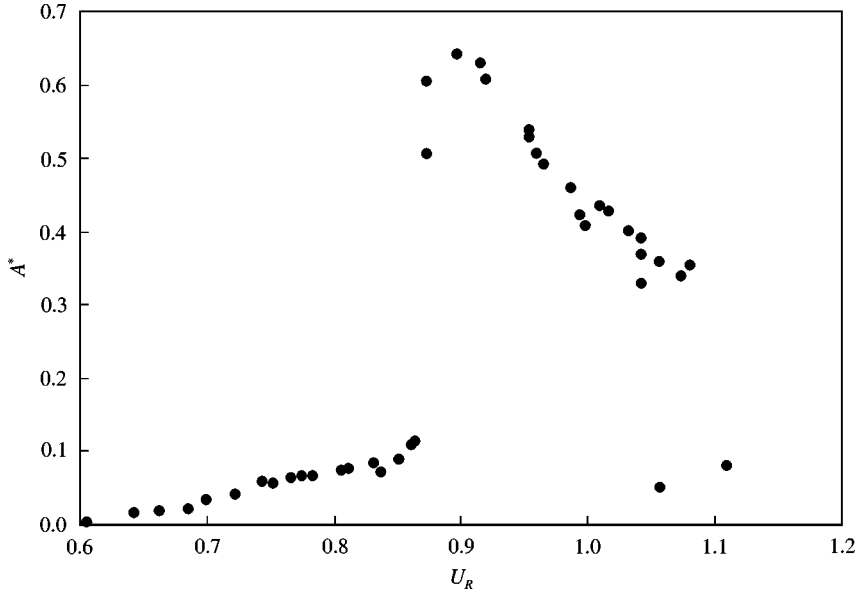

Figure 6. Amplitude plotted against reduced velocity for $m^* = 28{\cdot}0$. For the value $U_R = 1$, $b^* = 0{\cdot}39$, $k^* = m^*$, and $\mathrm{Re} = 23 \times 10^3$. Experiments of Gharib (1999).

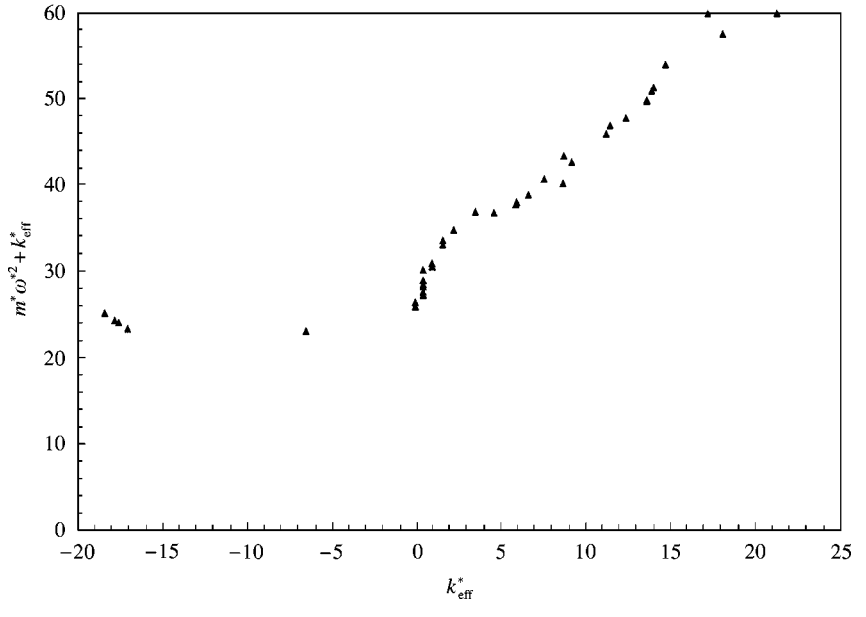

Figure 7. $m^*\omega^{*2} + \mathrm{k}^*_{\mathrm{eff}}$ or m^*/U_R^2 plotted against effective elasticity for the case $m^* = 28{\cdot}0$. Same experiment as in Figure 6.

parameters, mass ratio, m^*, reduced velocity, U_R, and mass damping, $m^*\zeta$ for transverse oscillations of an elastically mounted body. Body geometry and Reynolds number remain as additional parameters in either case.

As noted in SLR, the results of a traditional experiment performed at a given m^* may be used to predict the results for other m^*. This is so because, in a given experiment in which

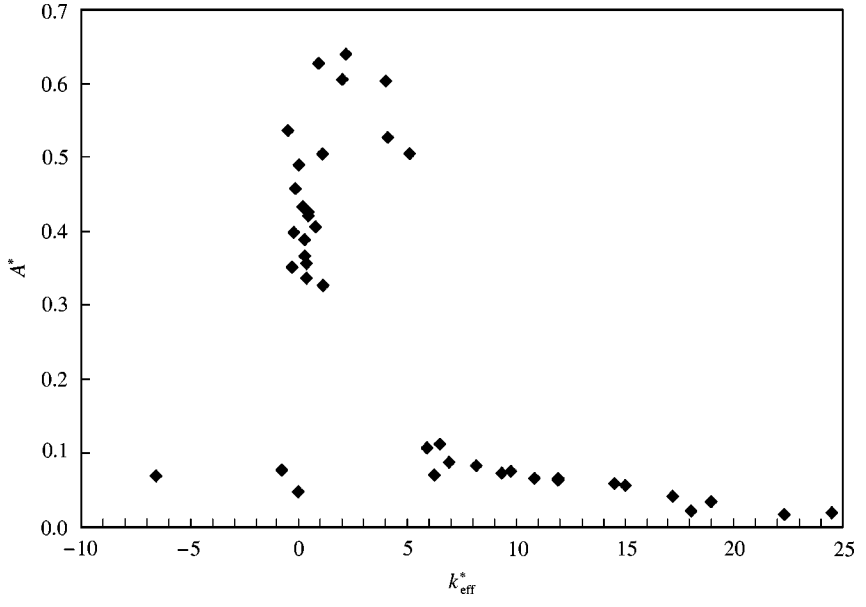

Figure 8. Amplitude plotted against effective elasticity for $m^* = 28{\cdot}0$. Same experiment as in Figure 6.

U_R is varied, the unifying parameter

$$k^*_{\text{eff}} = k^* - m^*\omega^{*2} = m^*/U_R^2 = m^*\omega^{*2} \tag{10}$$

also takes on all values of interest. In particular, we have shown that the branching of solutions, often observed in traditional experiments, is a consequence of the response frequency dependence on k^*_{eff}, which itself is dependent on the response frequency. For the limited computational and experimental data we have considered in this paper branching behavior is predicted and observed to occur only at higher m^*. The response, A^* versus U_R, is smooth at low m^*. This result appears to be at odds with the branching observed by Khalak & Williamson (1997) for $m^* = 2{\cdot}4(\pi/2) = 3{\cdot}7$ but could be due to effects of Reynolds number.

The possibility of formulating a unified description of the response, in terms of one parameter, k^*_{eff}, was facilitated by setting the damping b^* equal to zero in the numerical simulations, thereby ensuring that the spring and inertial forces are in line. A few simulations (in SLR) over a range of finite b^* show, not surprisingly, that amplitude is reduced ($\mathrm{d}A^*/\mathrm{d}b^* \simeq -0{\cdot}3$ for $b^* \ll 1$). Thus, the maximum value of amplitude for the unified solution, $A^* = 0{\cdot}59$ [Figure 1(a)], must be the maximum value for any combination of parameters, at Re = 100!

The relation of b^* to the conventional damping coeffieient ζ is given by $b^* = 2m^*\zeta/U_R$, i.e., it is equal to about twice the "mass-damping parameter" $m^*\zeta$ (since $U_R \sim 1$) that has been used to determine maximum values of amplitude, starting with investigations by Griffin & Ramberg (1982). Indeed, $A^* \to A^*_{\max}$ for $b^* \to 0$, as found by those and other investigators. The maximum value of amplitude, however, depends on Reynolds number. This is evident from the result of Khalak & Williamson (1997, 1999) and of Gharib (1999); values of A^* as high as 1·2 have been observed.

Among the issues that need further investigation is that of modeling vortex-induced vibration. It seems that modeling efforts could benefit by considering the unified description

presented in this paper and SLR. But it will still be a challenging task given, e.g., the counter-intuitive relation between amplitude and transverse force coefficient discussed above. Another item that needs further consideration is nonsinusoidal response and how such a response might be considered within the framework of the unified description. As noted above, aperiodic behavior does occur under certain conditions. In the computational study, for example, the response becomes modulated in what would be the range, $3 < k^*_{\mathrm{eff}} < 5$.

ACKNOWLEDGEMENTS

Thanks to Ms Lorena Barba for providing the results of her numerical simulations prior to publication and for her assistance in preparing the figures. We have also benefited greatly from interactions with Dr Mohammad Gharib and with Prof. Morteza Gharib. This work has been supported by ONR Grant #N00014-94-1-0793.

REFERENCES

BRIKA, D. & LANEVILLE, A. 1993 Vortex-induced vibrations of a long flexible circular cylinder. *Journal of Fluid Mechanics* **250,** 481–508.

FENG, C. C. 1968 The measurement of vortex-induced effects in flow past stationary and oscillating circular and D-section cylinders. M.A.Sc. thesis, University of British Columbia, Vancouver, BC, Canada.

GHARIB, M. R. 1999 Vortex-induced vibration, absence of lock-in and fluid force deduction. Ph.D. Thesis, California Institute of Technology, Pasadena, CA, U.S.A.

GHARIB, M. R., LEONARD, A., GHARIB, M. & ROSHKO, A. 1998 The absence of lock-in and the role of mass ratio. In *Proceedings of the 1998 Conference on Bluff-Body Wakes and Vortex-Induced Vibration* (eds P. W. Bearman and C. H. K. Williamson), Paper No. 24. Ithaca, NY: Cornell University.

GHARIB, M. R., SHIELS, D., GHARIB, M., LEONARD, A. & ROSHKO, A. 1997 Exploration of flow-induced vibration at low mass and damping. In *Proceedings of Fourth International Symposium on Fluid-Structure Interaction, Aeroelasticity, Flow-Induced Vibration, and Noise* (eds M. P. Païdoussis *et al.*), Vol. 1, pp. 75–81. New York: ASME.

GRIFFIN, O. M. & RAMBERG, S. E. 1982 Some recent studies of vortex shedding with application to marine tubulars and risers. *ASME Journal of Energy Research and Technology* **104,** 2–13.

KHALAK, A. & WILLIAMSON, C. H. K. 1997 Fluid forces and dynamics of a hydroelastic structure with very low mass and damping. *Journal of Fluids and Structures* **11,** 973–982.

KHALAK, A. & WILLIAMSON, C. H. K. 1999 Motions, forces and mode transitions in vortex-induced vibrations at low mass-damping. *Journal of Fluids and Structures* **13,** 813–851.

KOUMOUTSAKOS, P. & LEONARD, A. 1995 High-resolution simulations of the flow around an impulsively started cylinder using vortex methods. *Journal of Fluid Mechanics* **296,** 1–38.

SHIELS, D., 1998 Simulation of controlled bluff body flow with a viscous vortex method. Ph.D. thesis, California Institute of Technology, Pasadena, CA, U.S.A.

SHIELS, D., LEONARD, A. & ROSHKO, A. 2001 Flow-induced vibration of a circular cylinder at limiting structural parameters. *Journal of Fluids and Structures* **15,** 3–21.

APPENDIX: ADDED MASS

The "apparent" or "added mass" of an accelerating body is equal to the reactive force which the body exerts on the fluid in which it is immersed divided by the acceleration. Alternatively, it is equal to the impulse given to the fluid during an incremental change of body velocity divided by that incremental velocity. For the circle (cylinder in two-dimensional flow) or sphere, the impulse is aligned with the velocity change, but not in general, and then the ratio of impulse to velocity, i.e., the apparent mass, is a tensor quantity. These properties are well known from textbook derivations which are usually obtained for irrotational flow

and so it is not as well known that the resulting definitions are applicable more generally, e.g., in separated flows such as those that occur in problems of flow-induced vibration. As a result, empirical relations are sometimes introduced into models, unnecessarily. This assertion perhaps becomes obvious on noting that, in incompressible flow, an incremental velocity ΔV instantaneously generates a potential velocity field, proportional to ΔV, which is superimposed on the existing velocity field, whatever that may be, and that is why the conventional derivation based on irrotational flow is successful. But an alternative derivation, which addresses the vorticity field explicitly, may be more convincing. Here, we derive the result specifically for a circular cylinder.

The force $\mathbf{F}_b$ on the cylinder in two-dimensional flow can be calculated from the following relation (Koumoutsakos & Leonard 1995):

$$\mathbf{F}_b = \rho \frac{\mathrm{d}}{\mathrm{d}t} \int_{\text{fluid}} \boldsymbol{\omega} \times \mathbf{x} \, \mathrm{d}A + \rho A_B \frac{\mathrm{d}\mathbf{U}}{\mathrm{d}t}. \tag{A.1}$$

[in equation (21) of Koumoutsakos & Leonard, the sign of the first term is incorrect.] Using polar coordinates (r, θ), with origin at the center of the circle and θ measured from the direction of acceleration, $\mathrm{d}V/\mathrm{d}t$, the force F in that direction is

$$F = \frac{\mathrm{d}}{\mathrm{d}t} \int_a^\infty \int_0^{2\pi} r\omega_z \sin\theta r \, \mathrm{d}r \, \mathrm{d}\theta + \rho\pi a^2 \frac{\mathrm{d}V}{\mathrm{d}t}. \tag{A.2}$$

Vorticity is found only in the boundary layer and wake of the body. Unsteadiness of that vorticity results in unsteadiness of F, even if the body is stationary. However, independently, during acceleration *new* vorticity is generated at the surface of the body, and instantaneously creates a potential velocity field as noted above; its contribution to the force integral is the only contribution connected with the body acceleration and it uniquely defines the added mass. This contribution to the integral in equation (A.2) may be evaluated by noting that the new vorticity is contained in a singular layer whose strength $\gamma(\theta) = \lim_{\delta\to 0} \int_a^{a+\delta} r^2\omega_z \, \mathrm{d}r = \lim_{\delta\to 0} \int r^2(-\partial u_\theta/\partial r) \, \mathrm{d}r = a^2(-2\Delta V \sin\theta)$. The last term in parenthesis is the velocity along the cylinder surface (i.e., at the edge of the singular vorticity layer) due to an incremental velocity ΔV of the cylinder. Using this in equation (A.2) to complete the evaluation of the integral, we get

$$F = -2\rho\pi a^2 \frac{\mathrm{d}V}{\mathrm{d}t} + \rho\pi a^2 \frac{\mathrm{d}V}{\mathrm{d}t} = -\rho\pi a^2 \frac{\mathrm{d}V}{\mathrm{d}t}. \tag{A.3}$$

(Note that for a stationary body [$U_b = 0$ in equation (A.1)] in an accelerating stream, the result will be $F = -2\rho\pi a^2 \, \mathrm{d}V/\mathrm{d}t$.)